Separated flow behind a backward-facing step. Part II. Experimental and numerical investigation of a turbulent flow.

Tatiana G. Elizarova[1], **Eugene V. Shilnikov**[1],
Régine Weber[2], **Jacques Hureau**[2]

[1] Inst. for Math. Modelling, Russian Academy of Sciences,
Miusskaya Square, 4a, Moscow 125047, Russia, elizar@imamod.ru
[2] Lab. de Mécanique et d'Energétique, Polytech'Orláns,
8, Rue Léonard de Vinci, 45072 Orléans Cedex 2, France, Regine.Weber@univ-orleans.fr,
Jacques.Hureau@univ-orleans.fr

We present the results of an experimental and numerical investigation of a turbulent flow over a backward-facing step in a channel. Experimental data are visualized using a Particle Image Velocimetry (PIV) device. As a mathematical model we used quasi-hydrodynamic (QHD) equations. We have carried out numerical modeling of the flow for three configurations that were also studied experimentally. The computed flow proved to be non-stationary. The averaged flow in the separation zone is in a good agreement with the experimental data.

1 Introduction

In this paper we compare the results of the experimental and numerical investigation of a turbulent flow with medium Reynolds numbers over a backward-facing step in a channel.

An adequate description of a non-stationary flow in the separation zone behind the backward step is a considerable problem both in experimental and numerical aspects. As far as the numerical methods are concerned, a great variety of approaches are currently proposed to describe a turbulent flow. From the experimental point of view, visualization is a difficult task due to the great differences in the velocity of the flow in the main stream and in the separation zone, which hampers simultaneous visualization of the flow above the step and in the separation zone. Additional dificulties arise from the nonstationary character of the flow.

At present there is a significant number of computations of flows over a backward-facing step in a channel using the averaged Navier-Stokes equations (see [1] - [8] and literature cited there). The length of the separation zone related to the height of the step L_s/h in turbulent regime practically does not depend on the Reynolds number and varies - according to estimations [1] - [8] - from 5 to 8 depending on the geometry of the problem.

Averaged equations aimed at obtaining stationary numerical solutions, but the ambiguity in choosing the parameters of the model may lead to non-stationary flows behind a step as well [6]. Meanwhile even in the case of a developed turbulent flow the question of validity of the turbulence model remains. Non-stationary turbulent flow regimes may be obtained using the LES (Large-Eddy Simulation) or DNS (Direct Numerical Simulation) approaches, e.g. [9] - [11]. At present there is a number of results in numerical 3D-simulation of flows over a backward-facing step (e.g. [12]).

The experiments described in this paper were carried out at LME in a wind-tunnel; attention was mainly paid to the flow in the symmetry plane. The experimental device was adapted for low velocity flows with relatively small Reynolds numbers, that, nevertheless, provided turbulent regimes behind a backward-facing step. The results were obtained with a Particle Image Velocimetry (PIV) device.

The numerical simulation of the flow was done on the basis of quasi-hydrodynamic (QHD) equations, proposed by Yu.V. Sheretov [13]. QHD equations differ from the Navier-Stokes system in additional dissipative terms of a second order in space.

The scheme of the investigated flow is presented in Fig. 1. The Reynolds number is given by $Re = (U_0 h)/\nu$, where U_0 – is the average gas velocity in the entrance section of the channel, h – is the height of the step, ν – is the kinematic viscosity of the medium. The first computational and experimental results were presented in [14]-[17]. A brief description of the QHD system and its testing by computing a laminar backward-facing flow is given in the part I of the present publication [18].

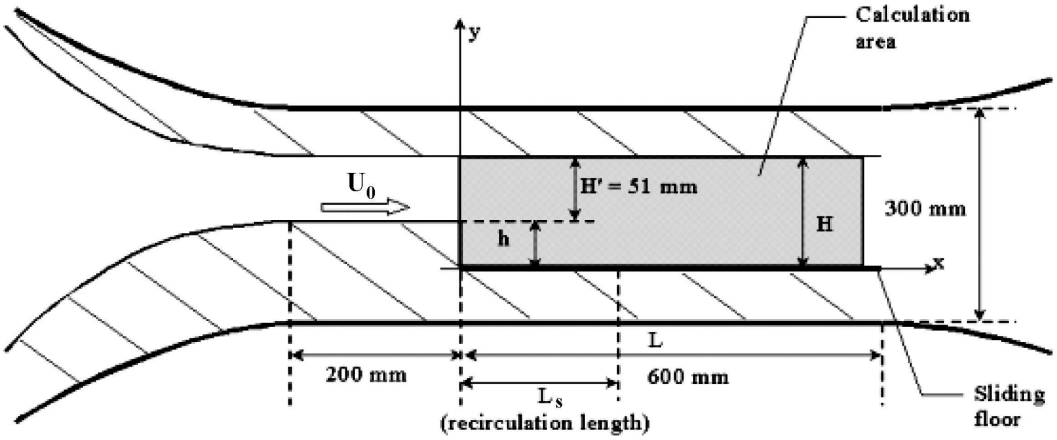

Figure 1: Wind tunnel section and notations.

2 Experimental setup

2.1 Wind tunnel

The experimental results have been obtained in an open air-driven wind-tunnel at LME (Orléans, France). The existing square section (300×300 mm) has been adapted to present a two-dimensional backward-facing step with adjustable step height. The width and the length (800 mm) of the test section were not modified. The electrically powered fan allowed us to obtain velocities of about 1 to 80 m/s in the non-adapted test section without any obstacle. Previous works published in the literature about this subject [1] pointed out that the reattachment length L of the flow behind the step varies with the Re number and the height h of the step: L can be twenty times larger than h. So, to be able to visualize the whole flowfield (and especially the reattachment area), the test section height H' upstream of the step was fixed to 51 mm and we have considered different step heights between 12 mm and 50 mm. The length of the test section before the step is 200 mm, which allows the flow to be fully developed. The mean velocity obtained is approximately 1.4 m/s (as checked with a two-components hot-wire anemometer). The mean turbulent ratio then measured is less than 0.85 % ahead of the step. One wall is transparent, for direct visualization, and the other ones are black. A laser sheet enters the wind tunnel section through a glass window in the upper wall.

2.2 Particle Image Velocimetry (PIV)

The experimental data generated are the two-dimensional components of the velocity behind the backward-facing step. An oil generator, placed at the entrance of the tranquillization room (velocity about 0.01 m/s), is used to generate and supply tracer particles. The mean diameter of the particles is about 1 μm. The laser sheet is generated by a double-oscillator laser: a Nd/Yag laser (Spectra Physics 400) adjusted on the second harmonic and emitting two pulses of 200 mJ each ($\lambda = 532$ nm), at a repetition rate of 10 Hz. The laser sheet is developed with an optical arm containing mirrors. Lenses allow us to obtain a laser sheet with a divergence of about 60° and with a thickness of about

1 mm in the vicinity of the step. For the present experimental data, the flow images are picked up by a PIVCAM CCD camera with 1008×1016 sensor elements, placed perpendicularly to the laser sheet. The laser pulses are synchronized with the image acquisition by a TSI synchronizer system driven by the InSight-NT^{TM} software. As stated previously, the reattachment length can be as long as twenty times the height of the step. The aim of these experimental measurements is to obtain the mean flow behind the step, so we have chosen to decompose the flow area into several visualized areas (80×80 mm or 135×135 mm) to ensure a good precision in the wake of the step. This is only possible because the mean velocity field is studied. These sub-areas overlap by about 10 mm. For all the results presented here, the PIV recordings are divided into interrogation areas corresponding to 64×64 pixels. For data post-processing, the interrogation areas overlap by 50%. The local displacement vector is determined for each interrogation area by statistical methods (auto-correlation). The projection of the local flow velocity vector onto the laser sheet plane is calculated by InSight using the time delay between the two illuminations ($\Delta t = 1$ ms) and the magnification at imaging. The post-processing used here is very simple – no more than a velocity range filter.

3 Numerical modeling of turbulent flows

Numerical modeling of flow over a backward-facing step is carried out in accordance with the experimental parameters for the Reynolds numbers $Re(h) = 4667$, 4012, 1667 and the ratios $h/H = 0.5$, 0.44, 0.33 respectively.

The flow in the wind-tunnel is air

at room temperature, atmospheric pressure with entrance velocity $U_0 \sim 1.2$ - 1.4 m/sec. The sound velocity in air under normal conditions equals $c_s = 340$ m/sec. Because $U_0/c_s \sim 0.003$, we apply the approximation of a viscous incompressible isothermal flow [19]. Experimental visualization is done in the symmetry plane; therefore, we use a plane two-dimensional model of a flow in the numerical computations.

These simplifying assumptions permit us to apply the finite difference algorithm described and tested in [18] and allowing for non-stationary flows. Unlike [18], we now specify a plane velocity profile in the entrance section, that coincides with the conditions of the experiment.

Numerical calculations were performed using the quasi-hydrodynamic (QHD) equations that differ from the Navier-Stokes ones by additional dissipative terms. These terms include a multiplying factor τ, - relaxation (smoothing) parameter, which has a dimension of time. For laminar flows, τ is related to the molecular viscosity coefficient. For turbulent flows the value of τ is no longer related with molecular viscosity and must be adjusted to fit the general flow features. The theory of QHD equations is presented in [13] and briefly described in [18].

The results of computations are gathered in Tables 1–3 and are presented in Figs. 2–16. Additional computations may be found in [16]. Tables contain the serial number of computation (run), the dimensionless value of the smoothing parameter τ, the spatial grid step, the number of grid nodes $N_y \times N_x$, the dimensionless computing time T_0 and the reference to the figures that illustrate this computation. Spatial grids are uniform and have equal steps in both directions ($h_x = h_y$). Parameter τ varies widely. The dimensionless time step in all presented variants is equal to $\delta t = 10^{-4}$.

Velocity and pressure fields were recorded every 5000 steps, that is, with a time interval $\Delta t_1 = 0.5$. The velocity components in four particular locations behind the step were recorded every 500 steps, i.e., with a time interval $\Delta t = 500\,\delta t = 0.05$. Energy spectra of the velocity components pulsations were computed for $Re = 4667$ and $Re = 4012$ according to the algorithm described in the Appendix.

Computations were carried out in the dimensionless variables defined in [18]. For $Re = 1667$, we had $H = 71$ mm, $U_0 = 1.25$ m/s, and the dimensionless time $\tilde{t} = 1$ corresponding to $H/U_0 = 0.056$ s; for $Re = 4012$ and 4667, this variable corresponded 0.063 s and 0.072 s, respectively.

3.1 Variant $Re = 4667$

The major computational work for the proper choice of the smoothing parameter τ was carried out for $Re = 4667$ (Tab.1, Figs.2–8).

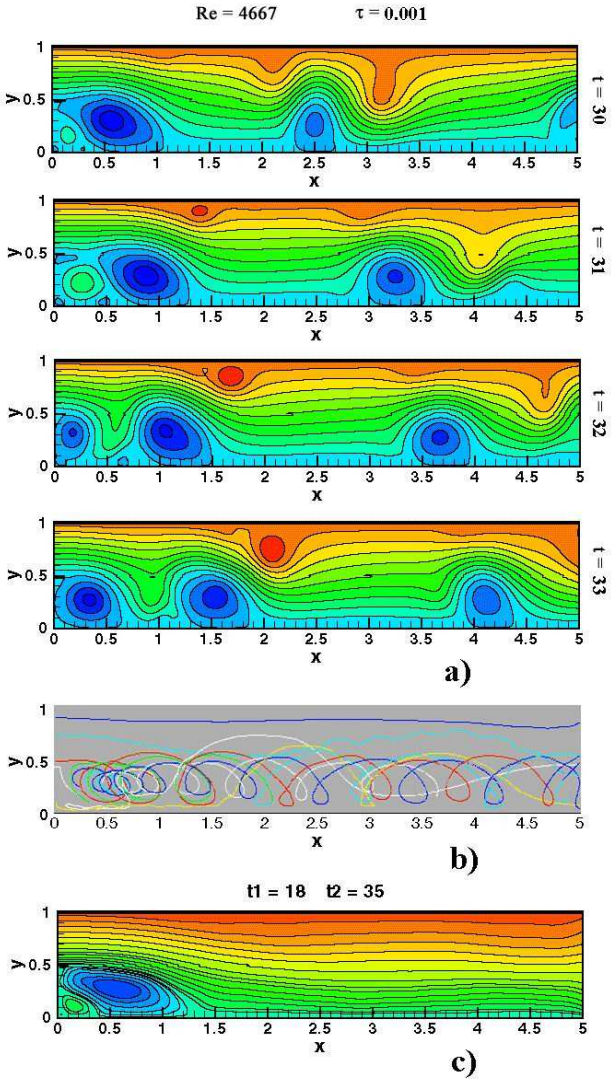

Figure 2: Instant stream functions (a), trajectories of fluid particles (b), averaged flow field (c) for Re=4667, run 2.

Fig. 2a demonstrates the sequences of the stream function isolines, computed according to algorithm [18], at four successive times (indicated at the right of the figure. A single vortex appears behind the step; its length increases and then the single large vortex splits into several small ones that rotate in opposite directions. These smaller vortices are torn away from the main one and carried down the flow till they leave the computational domain.

Fig. 2b demonstrates the trajectories of the fluid particles; the Fig. 2c demonstrates the velocity field time-averaged between t_1 and t_2 (values indicated in the figure). The averaged velocities u_x^{av} and u_y^{av} in every computational point are computed as

$$u_x^{av} = \frac{1}{t_2 - t_1} \int_{t_1}^{t_2} u_x(t)dt, \quad u_y^{av} = \frac{1}{t_2 - t_1} \int_{t_1}^{t_2} u_y(t)dt.$$

N run	τ	$h_x = h_y$	$N_y \times N_x$	L	T_0	Figure number
1	0.0001	0.0125	80 x 400	5	20	–
2	0.001	0.00833	120 x 600	5	40	Fig.2
3	0.001	0.0125	80 x 400	5	20	–
4	0.05	0.00833	120 x 600	5	120	Figs.3 - 8
5	0.05	0.0125	80 x 400	5	120	
6	0.1	0.0125	80 x 600	7,5	40	–

Table 1: Computations for $Re = 4667$, $H = 101\,\text{mm}$, $U_0 = 1.40\,\text{m/s}$, $h/H = 0.5$.

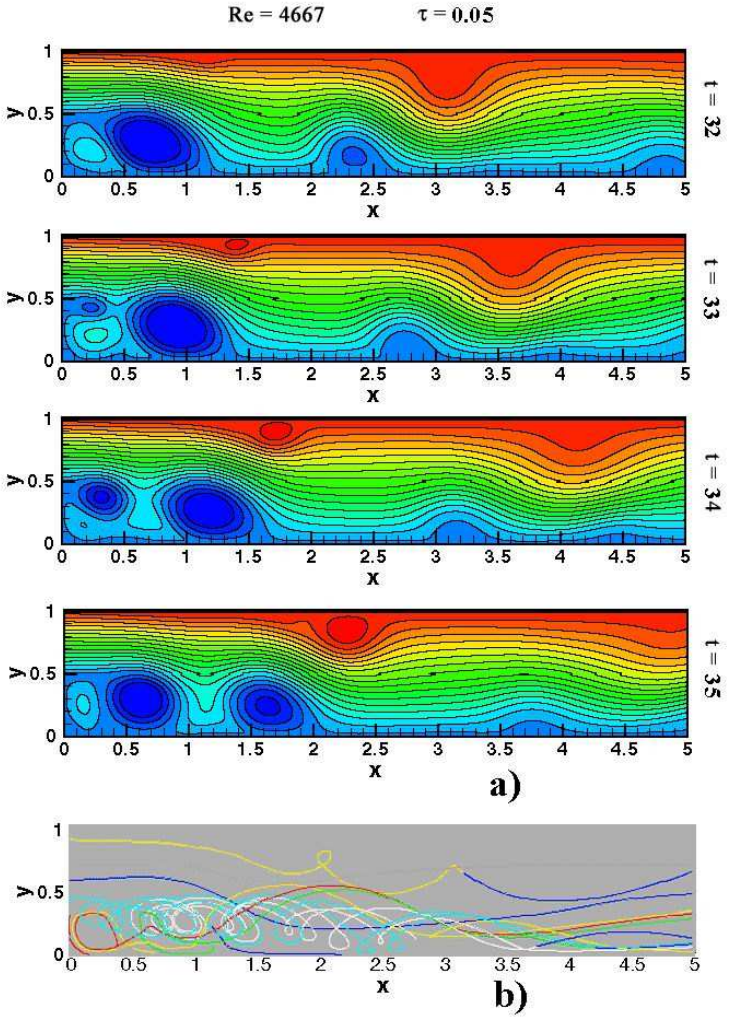

Figure 3: Instant stream functions (a) and trajectories of fluid particles (b) for $Re = 4667$, run 4.

The stream function is then computed using the averaged values. This procedure is correct due to the commutativity of temporal averaging and spatial differentiation.

From Fig. 2 it is easily seen that for a quickly changing flow the flow pattern looks essentially different at four different times. The recirculation flow is well seen only on the stream functions

that are constructed using the averaged velocities (Fig. 2c). The size of the separation zone equals $L_s/h \sim 3$, which is twice less than observed experimentally. The same mean size of the separation zone is obtained in computations on a twice less accurate spatial grid with the same $\tau = 0.001$ (run 3) and also with asmaller $\tau = 0.0001$ (run 1). In the last case the time step was equal to $\delta t = 10^{-5}$. Therefore, for $\tau \leq 0.001$ a quasi-periodical flow is formed behind the step, and its shape rather weakly depends on the value of τ and on the size of the spatial grid. In these computations the separation zone proves to be smaller than the one observed in experiments.

Computations 4 and 5 correspond to $\tau = 0.05$. In Fig. 3–8 we demonstrate the results of computation 4. As well as in other computations, instantaneous pictures of the stream function (Fig. 3a) look much the same and strongly resemble those in Fig. 2a. The trajectories of fluid particles (Fig. 3b) do not exhibit a recirculation zone.

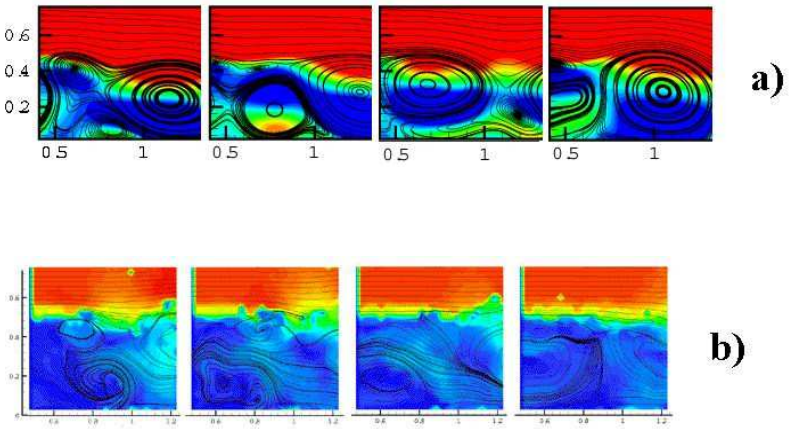

Figure 4: Fragments of the averaged flow field: computational (a) and experimental (b).

In Fig.4a we show computed pictures of a flow fragment behind the step. This fragment corresponds to the region 0 - 0.75 along the ordinate and 0.4 - 1.3 along the abscissa. Each numerical pattern is constructed from the instantaneous velocity vectors, averaged over time intervals $t_2 - t_1 = 0.015$ (1 ms). We give 4 successive pictures starting from times $T_1 = 70$, $T_2 = 71,5$, $T_3 = 73$ and $T_4 = 74,5$. So the numerical flowfields are obtained at a time interval of 1.5 (0.1 s, frequency 10 Hz).

Fig.4b shows the time sequence of experimental flowfields obtained at a frequency of 10 Hz in the same part of the flow domain behind the step. The velocity fields are obtained by intercorrelation between two images acquired with an interval time of 1 ms, that corresponds with the time delay between two laser illuminations.

Averaging intervals in Figs.4a and 4b are approximately the same. Experimental and computational portraits of the flow both demonstrate a chaotic non-stationary kind of flow, and the typical sizes of inhomogeneities obtained from computations agrees with the ones observed experimentally.

Fig. 5 we show the computed flow fields, averaged over larger time intervals ($t_2 - t_1$ equals 0.5 - 2 s). In Fig. 6 we show the experimental flow fields averaged over intervals of 8-10 seconds. One can see the good agreement - both in size ($L_s/h \sim 6$) and in structure of the separation zone in these averaged pictures. In both cases the averaged pictures depend on initial time t_1 and integration time $t_2 - t_1$, but this dependence is weak, because the averaging time is essentially larger than the typical time of velocity fluctuations.

Fig. 7 illustrates the time dependence of velocity components u_x and u_y as functions of time at three points located behind the step and far from the wall. The flow is essentially non-stationary and quasi-periodical. The general features of these curves depends weakly on the location of the points.

The pulsation spectra $E(k)$ of the velocity component u_x at three spatial points are plotted in Fig. 8. The mentioned spectra may be considered as reliable up to $k \approx 240$. The $k = 0$ harmonic

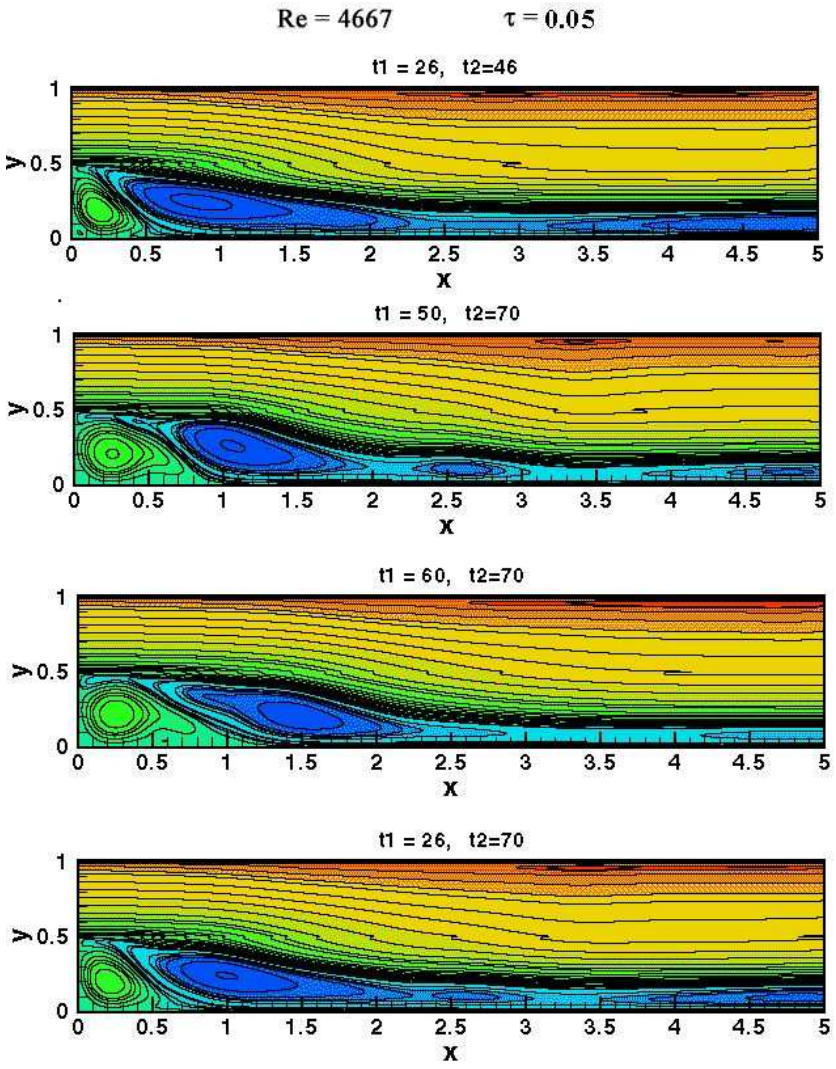

Figure 5: Averaged flow fields, computation, $Re = 4667$.

is absent because it is related to the average velocity $\bar{u}$. Fourier series expansion is carried out after completing the initial relaxation to stable oscillations during the time interval from $t = 40$ to $t = 120$. The main oscillation frequencies and the decrease of amplitude for the harmonics at large and small values of k are easily seen.

The results of computations 4 and 5 on different spatial grids were shown to be close to one another.

Computation 6 is carried out with a large value of the smoothing parameter τ. The structure of the flow proves to be non-physical - the non-stationary separation zone behind the step grows indefinitely and reaches the right border of the computation zone. In this case the velocities in the flow change slowly and the trajectories of the fluid particles are close to the streamlines. The averaged flow is of no interest in this computation. Additional computations and pictures illustrating them can be found in [16].

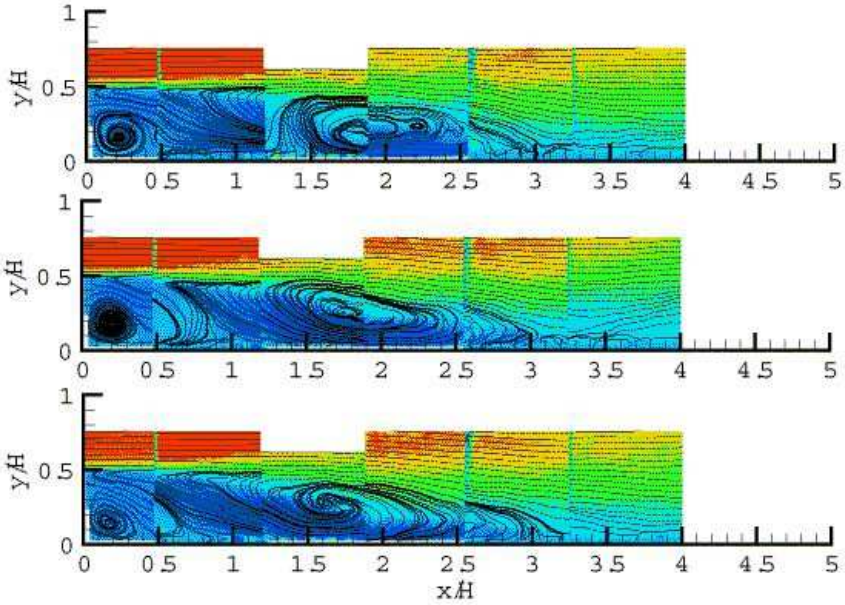

Figure 6: Averaged flow fields, experiment, $Re = 4667$.

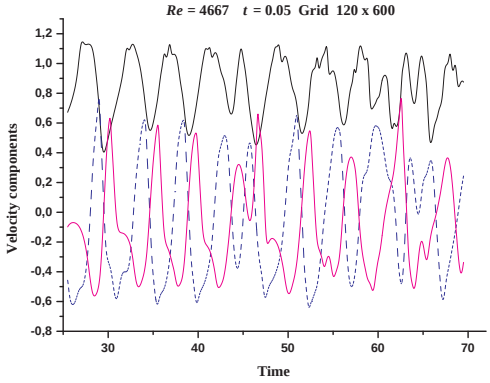

Figure 7: Fragment of temporal evolution of the velocities, computation, $Re = 4667$.

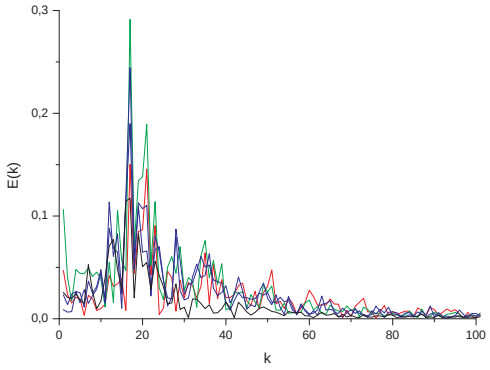

Figure 8: Velocity pulsation spectrum $E(k)$, computation, $Re = 4667$.

3.2 Variant $Re = 4012$

Computation results for this variant in general repeat those obtained before. In run 1 (see Table 2) we obtain a non-stationary solution with a separation zone length ($L_s/h \sim 2$) smaller than the experimental one.

N run	τ	$h_x = h_y$	$N_y \times N_x$	L	T_0	Figure numbers
1	0.001	0.0125	80 x 400	5	20	–
2	0.05	0.00833	120 x 600	5	200	Figs.9 - 14

Table 2: Computations for $Re = 4012$, $H = 92\,\text{mm}$, $U_0 = 1.45\,\text{m/s}$, $h/H = 0.44$.

In computation 2 with $\tau = 0.05$ we get pictures of the flow averaged over $t_2 - t_1 = 0.015$ (see Fig. 9a). In this figure, we show 8 successive pictures starting from T=154 with a time interval 1.5, that corresponds to a frequency of 10Hz. The corresponding experimental flow fragments are given in Fig. 9b starting from time $t_1 = 0.4\,\mathrm{s}$ with an acquisition rate equal also to 10Hz. Both starting points are chosen arbitrarily. Both calculated and experimental flow fields exhibit a chaotic non-stationary character.

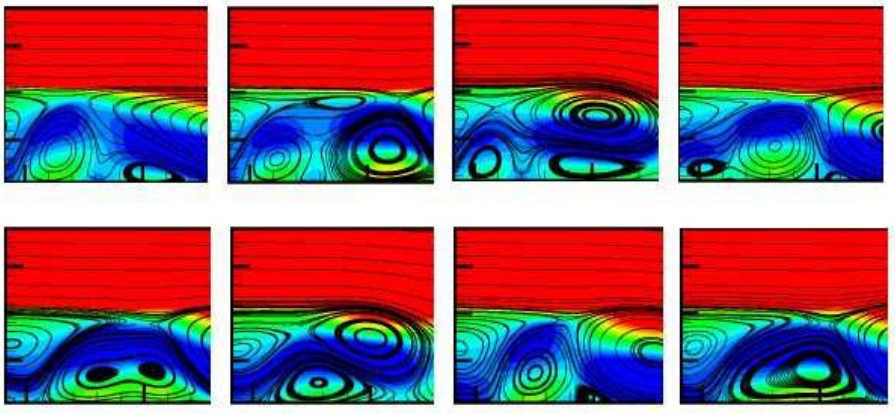

a)

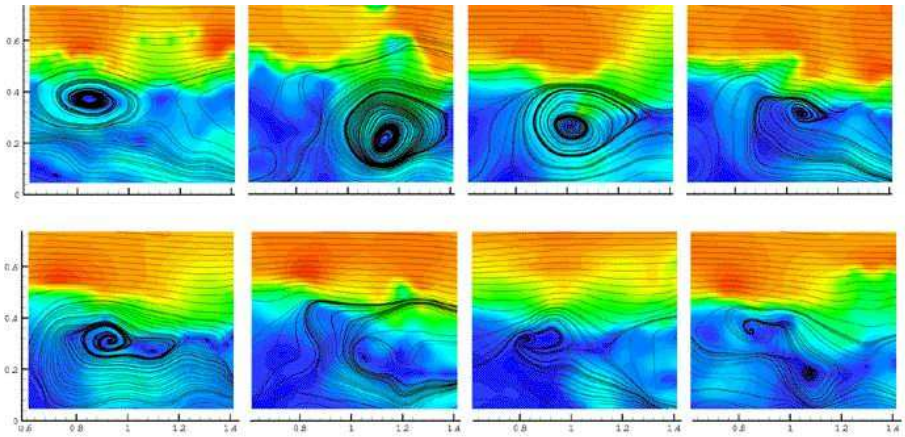

b)

Figure 9: Fragments of the averaged flow field: computational (a) and experimental (b) for $Re = 4012$.

In Fig. 10 we demonstrate the streamlines, averaged over long time intervals and constructed in the same way as in [18]. In Fig. 11 the corresponding experimental pictures of the flow in the separation zone are shown over a background color that represents the velocity component u_x.

Fig. 12 depicts the time evolution of the velocity components behind the step. It demonstrates quasi-periodical oscillations. Figs. 13 and 14 show the energy spectrum of pulsations of the velocity components in linear and logarithmic scales, respectively. The last one contains the dependence $E(k) \sim k^{-5/3}$ (Kolmogorov-Obukhov law in spectral form) [19]. This law of the kinetic energy dissipation is typical for well-developed turbulent flows. It can be easily seen that the numerical

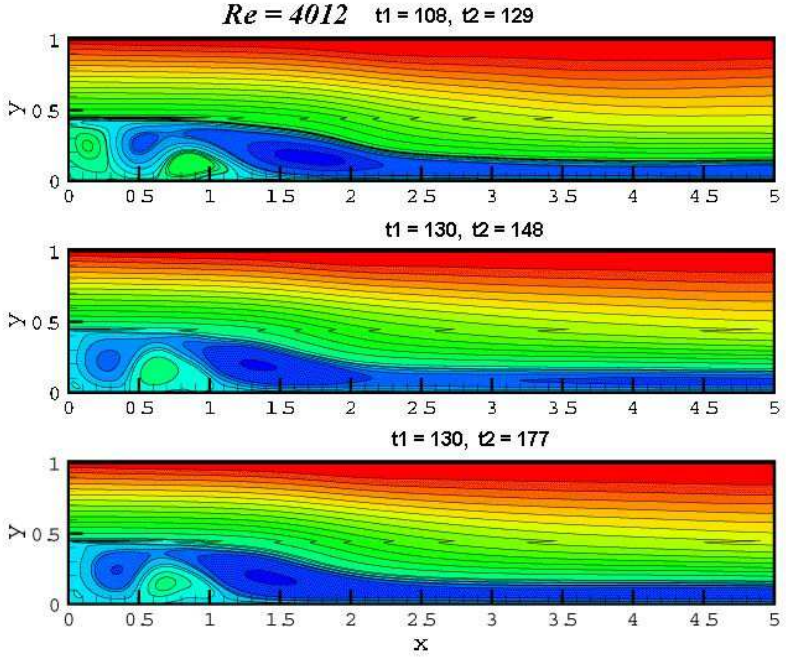

Figure 10: Averaged flow fields, computation, $Re = 4012$.

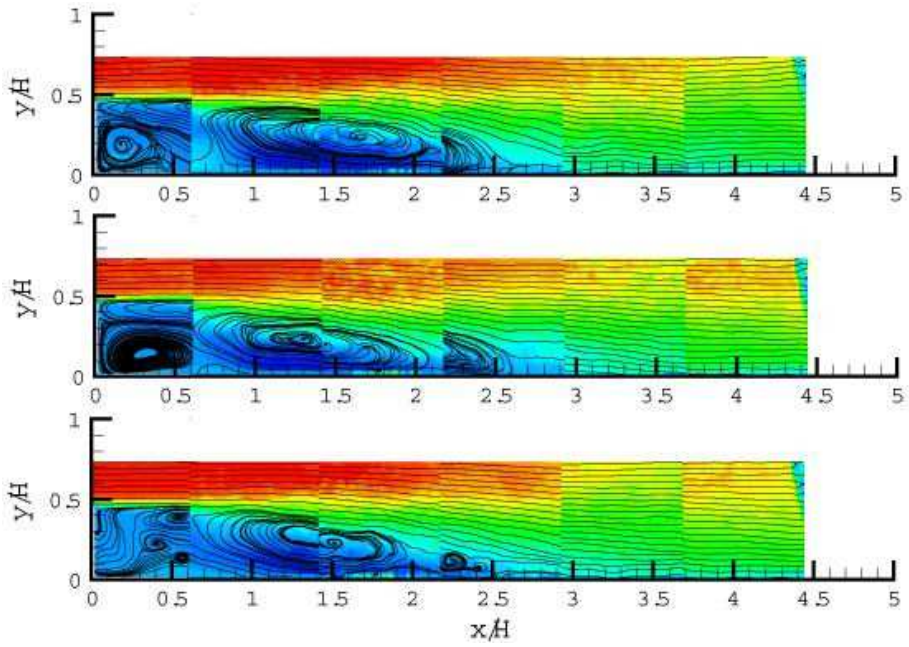

Figure 11: Averaged flow fields, experiment, $Re = 4012$.

energy spectrum in the frequency range, that agrees with the step of the spatial grid and with the time of computation T_0, coincides in general with the classical law of the decreasing of energy E with the growth of the wave number k.

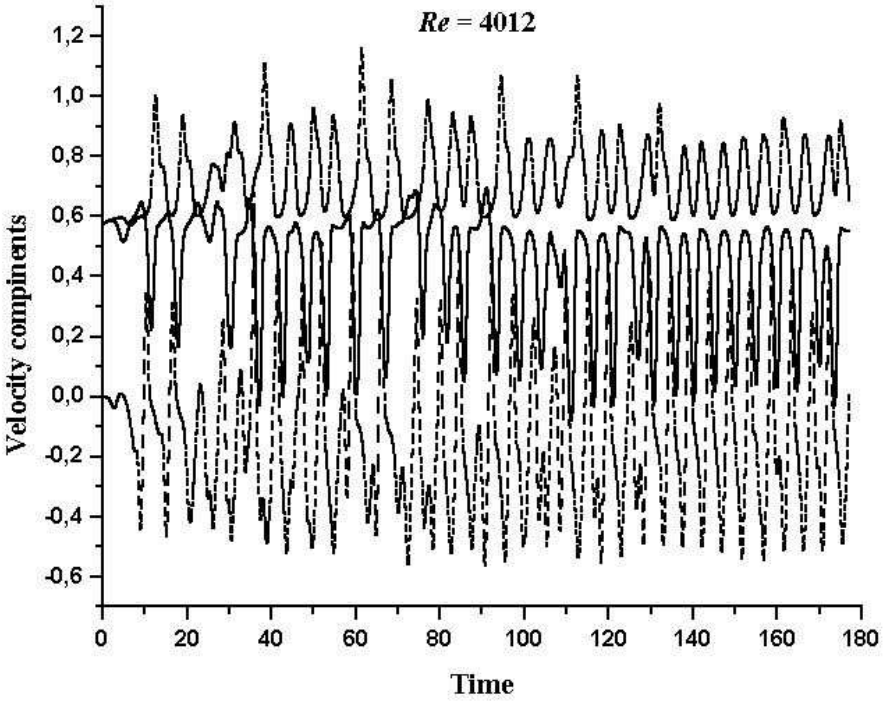

Figure 12: Temporal evolution of the velocity behind the step, computation, $Re = 4012$.

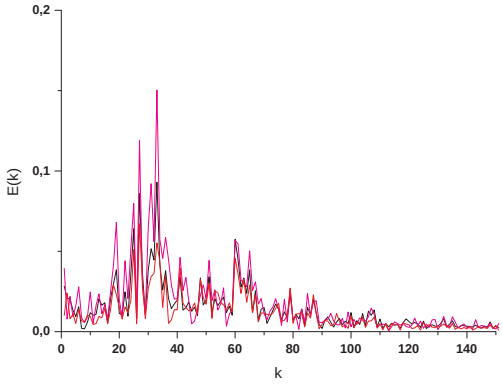

Figure 13: Velocity pulsation spectrum E(k), computation, $Re = 4012$.

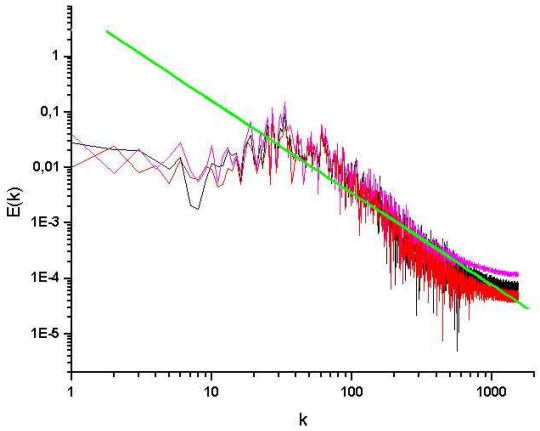

Figure 14: Velocity pulsation spectrum E(k), Logarithmic scale, computation, $Re = 4012$.

3.3 Variant $Re = 1667$

For $Re = 1667$ (see Table 3), in run 2, the length and the structure of the separation zone ($L_s/h \sim 6$) agrees with the experimental data. In run 1 ($L_s/h \sim 2,5$) the length of the separation zone proves to be smaller than in the experiment. In run 3 the numerical solution becomes non-physical - the separation zone grows indefinitely.

In Fig. 15a we show a series of the averaged stream function fields (run 2) The corresponding averaged experimental flow picture is shown in Fig. 15b. The size and the structure of the flow in the separation zone are in good agreement. Fig. 16 illustrates the temporal evolution of flow velocity components; it presents a quasi-periodical character.

N run	τ	h_x	$N_y \times N_x$	L	T_0	Figure number
1	0.001	0.0125	80 x 400	5	20	–
2	0.02	0.0125	80 x 480	6	160	Fig.15, 16
3	0.05	0.0125	80 x 480	6	60	–

Table 3: Computations for $Re = 1667$, $H = 71\,\mathrm{mm}$, $U_0 = 1.25\,\mathrm{m/s}$, $h/H = 0.33$.

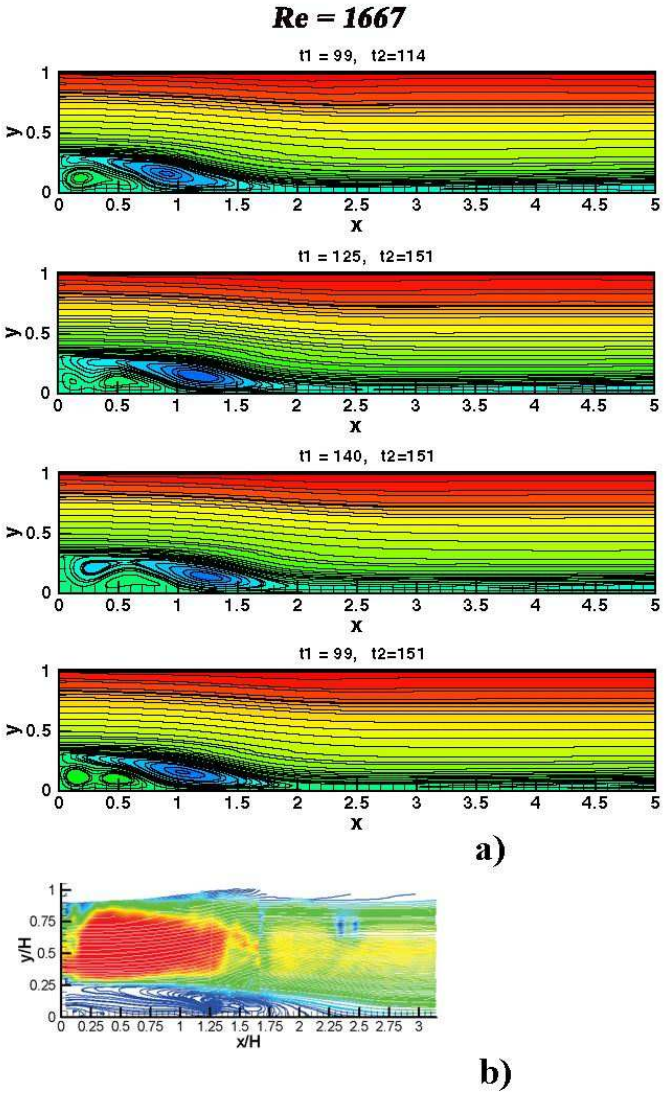

Figure 15: Averaged flow fields: computational (a) and experimental (b) for $Re = 1667$.

4 Discussion and conclusions

4.1 Relaxation parameter

Numerical computations are based on the QHD equations. They differ from the Navier-Stokes system by additional dissipative terms that contain a small parameter τ - relaxation (smoothing)

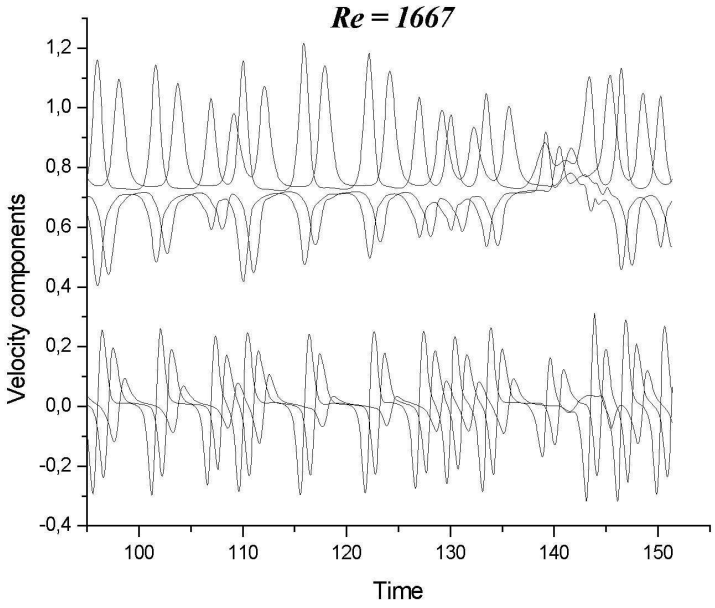

Figure 16: Temporal velocity evolution behind the step, computation, $Re = 1667$.

parameter. While computing turbulent flows, τ is chosen much larger than for computing laminar flows [18]. We manage to obtain the structure of the flow behind a backward-facing step by varying τ. The dependence of the averaged flow on τ proves to be relatively weak: in the variant $Re = 4667$ the length of the separation zone varied from $L_s/h \sim 3$ to $L_s/h \sim 6$, when τ was varied from 0.001 to 0.05. We should also mention that the parameter of relaxation τ is the only constant in the QHD model that must be adjusted to achieve agreement between numerical and experimental results.

A posteriori specification of the relaxation parameter on the basis of the flow field resembles to adjusting the turbulent viscosity in phenomenological models of turbulence. In these models the value of turbulent viscosity is not related with the coefficient of the molecular viscosity. This quantity is derived from experimental data, e.g., from the pulsation features of the flow or from its characteristic scales [19].

Agreement with the experimental data - as far as the length and the structure of the separation zone are concerned - is obtained in variants $Re = 4667$ and $Re = 4012$ for $\tau = 0.05$, and in variant $Re = 1667$ for $\tau = 0.02$. In dimensional form it corresponds to $3.6 \cdot 10^{-3}$ s, $3.2 \cdot 10^{-3}$ s and $1.12 \cdot 10^{-3}$ s respectively. In these cases the average length of the separation zone equals $L_s/h \sim 6$, and the position of the vortex centers coincide in computations and in experiments. The position of a secondary vortex located at the internal corner is also well described in the computations.

Mention, that in our calculations we have not seen the well-known anomaly of low-Reynolds-number (LRN) Reynolds-stress models (RSM) ([7], [8]), that is a spurious bending (backward curvature) of the dividing streamline at the reattachment point.

There remains the problem of a priori choice of the relaxation parameter in QHD equations for computing turbulent flows. Nevertheless, we may claim that $\tau \leq 1$, because the dissipative terms should be considerably smaller than the convective ones. In computations the minimal resolution scale is the step of the spatial grid. Therefore we may suppose that τ should be greater than the characteristic perturbation spreading time over one spatial step h_x; that is, $\tau \geq h_x/c_s$. Besides, for the problem under consideration, τ should be a fortiori greater than the averaging time, for which the velocity profile at the entrance of the channel may be considered as a flat. This time was not measured in the present experiments.

4.2 Flow visualization and time averaging intervals

The numerically observed type of the flow formation resembles the well-known Landau turbulence scenario [19]. This formation consists of the growth of initial perturbations that are suppressed by nonlinear media reactions. It leads to the appearance of a complex quasi-periodical motion, which seems to be turbulent[JCL6].

The computational time step δt that describes the variation of the nonstationary velocity field, is several orders of magnitude smaller than the time resolution of the experiments. So it is impossible to compare the numerical and experimental flow patterns directly, using instantaneous streamlines. The trajectories of the liquid particles, based on the stream-functions, are not suitable for the comparison with the present experiments. That is why we used averaged velocity fields when comparing numerical and experimental results.

We used two types of temporal intervals for visualizing the results of computations - large intervals for comparing global flow pictures and small intervals for comparing local "snapshots".

The averaging interval for global pictures equals $t_2 - t_1 = 10 - 50$ dimensionless units, that is, 0.5-3 s. This time interval exceeds largely the averaged period of the temporal velocity evolution (Figs. 7, 12 and 16). The number of averaged fields proves to be large enough, because the flow recording is done with the interval 0.5. In other words, the number of averaged velocity fields in computation approximately equals the number of averaged experimental images. It makes both averaging procedures equivalent in general. The obtained fields depend weakly on the beginning and length of the time averaging interval.

The averaging interval for comparing numerical and experimental "snapshots" equals to 0.015 dimensionless units, approximately 1 ms, which coincides with the time delay between the two illuminations - a gap between two pulses of the PIV installation. The numerical flowfields are obtained at a time interval ~ 0.1 s., to reproduce the experimental acquisition frequency of frequency ~ 10 Hz. The computational and the experimental averaged pictures in general look alike - both consist of small chaotically mixed non-stationary whirls that essentially depend on the choice of the temporal interval $t_2 - t_1$.

It is impossible to observe instant velocity fields experimentally. Therefore the question of validity of the computed instant velocity fields is physically senseless. At the same time numerical and experimental fields averaged over large and small time intervals prove to be consistent with each other.

4.3 Conclusions

In [18] the QHD equations were tested in a laminar flow simulation. There a relaxation parameter τ was determined by the molecular viscosity. In computations it was chosen as small as possible to provide the stability of the numerical computations. The stationary flow did not depend on its value. The initial oscillations of the solution faded during the time.

In the present paper we demonstrate that in the turbulent flow the initial perturbations do not fade and lead to the formation of non-stationary flow pattern, that resembles a periodical process.

This type of solution is observed for sufficiently small values of the dimensionless temporal relaxation parameter: $\tau \leq 0.1$.

The comparison of numerical solutions with experimental data is possible only on the basis of the averaged velocity fields. In this case the outlook of the averaged flow depends both on the value of the temporal relaxation parameter τ (which makes the difference between the QHD system and the Navier-Stokes equations) and on the chosen averaging interval.

In spite of considerable simplifications of the problem - using a two-dimensional model of the viscous non-compressible isothermal fluid - the results of computation are in good agreement with the present experiments.

We suppose that the numerical modeling of the turbulent flow over a backward-facing step by means of the QHD system is possible due to the additional (in comparison with the Navier-Stokes equations) dissipative terms that are small for the stationary flows and become not small for the non-stationary turbulent flows.

5 Appendix. Computing the spectrum of pulsations

The energy spectrum of the flow pulsations is computed on the basis of the time dependence of velocity components u_x and u_y. Let us write the velocity u_x as

$$u_x = \bar{u}_x + u'_x,$$

where $\bar{u}_x$ is the average velocity value, u'_x is its pulsation component. Then we apply the discrete Fourier transform to u'_x (for simplicity further on we omit primes). We present the pulsation component in form of a series

$$u_x = \sum_{k=1}^{N/2} (\frac{a_{k+1}}{N} cos\frac{2\pi lk}{N} + \frac{b_{k+1}}{N} sin\frac{2\pi lk}{N}).$$

To find the spectrum of pulsations let us compute Fourier coefficients:

$$a_{k+1} = 2\sum_{l=0}^{N-1} u_x^{l+1} cos\frac{2\pi lk}{N}, \quad b_{k+1} = 2\sum_{l=0}^{N-1} u_x^{l+1} sin\frac{2\pi lk}{N},$$

where u_x^l - is the value of the velocity u_x at i, j at time $l\Delta t$; N is the number of the considered records, k runs from 1 to $N/2$.

The energy spectrum is derived from these Fourier coefficients:

$$E(k) = a_k^2 + b_k^2.$$

The maximal value of $k = N/2$ corresponds to oscillations of period Δt. When the frequency of recordings is chosen, oscillations with higher frequencies are not allowed. But for proper resolution we need at least 4-5 points per period. Therefore the obtained spectrum can be considered as reliable for $k \leq N/8$.

For all variants of the present calculations, $\Delta t = 0.05$. For example, for $Re = 4012$, run 2, $T_0 = 200$, so the reliable range of k in Figs. 13, 14 is limited to $k \leq T_0/\Delta t/8 = 500$ approximately.

6 Acknowledgement

Authors are thankful to Jean-Claude Lengrand (Lab. d'Aerothermique du CNRS, Orleans) for the fruitful discussions and his contributions to the preparation of this article.

References

[1] Armaly B.F., Durst F., Pereira J.C.F., Schonung B.: Experimental and theoretical investigation of backward-facing step flow. J. of Fluid Mech. V. 127. pp. 473–496, 1983.

[2] Nallasamy M.: Turbulence models and their applications to the prediction of internal flows: a rewiew. Computers and Fluids. V. 15. N 2. pp. 151–194, 1987.

[3] Tong G.T.: Modelling turbulent recirculating flows in complex geometries. Computational Techniques and Applications: CTAC-83, Ed. Noye J., Fletcher C. Elsevier Science Publishers B.V. (North–Holland), pp. 653–668, 1984.

[4] Speziale C.G., Ngo T.: Numerical solution of turbulent flow past a backward facing step using a nonlinear K-ϵ model. Int. J. Eng. Sci., Vol.26, No 10, pp.1099–1112, 1988.

[5] Thangam S., Speziale C.G.: Turbulent Flow Past a Backward-Facing Step: A Critical Evaluation of Two-Equation Models. AIAA Journal, Vol.30, No 5, pp.1314–1320, 1992.

[6] Lasher W.C., Taulbee D.B.: On the computation of turbulent backstep flow. Int. J. Heat and Fluid Flow, Vol 13, No 1, pp.30–40, 1992.

[7] Shima N.: Low-Reynolds-number second moment closure without wall-reflection redistribution terms. Int. J. Heat and Fluid Flow. 1998, 1998. Vol.19, pp.549–555.

[8] So R.M.C., Yuan S.P.: A geometry independent near-wall Reynolds-stress closure. Int. J. Eng. Sci. 1999. Vol 37, pp.33–57.

[9] Fureby C.: Large Eddy Simulation of Rearward-Facing Step Flow. AIAA Journal, Vol.37, No 11, pp.1401–1410, 1999.

[10] Le H., Moin P., Kim J.: Direct numerical simulation of turbulent flow over a backward-facing step. J. Fluid Mech.1997. Vol 330, pp.349–374.

[11] Meri A., Wengle H., Schiestel R.: DNS and LES of a backward-facing step flow using 2nd- and 4th-order spatial discretization and LES of the spatial development of mixing of turbulent streams with non-equilibrium inflow conditions. Notes on Numerical Fluid Mechanics. Springer, V.75, 2000, pp. 268–287.

[12] Armaly B.F., Li A., Nie J.H.: Three-Dimensional Forced Convection Flow Adjacent to Backward-Facing Step. Journal of Thermophysics and Heat Transfer, Vol.16, No 2, p.222–227, 2002.

[13] Sheretov Yu.V.: Quasi-hydrodynamic and quasi-gasdynamic equations based mathematical modeling of liquid and gas flows. Tver: Tver State University 2000.

[14] Elizarova T.G, Kalachinskaya I.S., Weber R, Hureau J., Lengrand J.-C.: Ecoulement derrière une marche. Etude expérimentale et numérique. Laboratoire d'Aérothermique du CNRS, Orléans (Fr), R 2001 - 1 (2001).

[15] Elizarova T.G, Kalachinskaya I.S., Weber R, Hureau J., Lengrand J.-C.: Backward-facing step flow. Experimental and numerical approach. IUTAM Symposium "Unsteady separated flows". 8-12 April 2002, Toulouse, France. Abstracts.

[16] Elizarova T.G., Kalachinskaia I.S., Sheretov Yu.V., Shilnikov E.V. (2003): Numerical simulation of the backward-facing step flows. Prikladnaia Matematika i Informatika: Trudy Faculteta VMiK MGU. Moscow, MAKS Press, 2003, no. 14, pp. 85–118 (in Russian)

[17] T.G. Elizarova, E.V. Shilnikov, R. Weber, J. Hureau, J.-C. Lengrand.: Experimental and Numerical Investigation of the Turbulent Flow behind a Backward-Facing Step. Int. Conference on Boundary and Interior Layers (BAIL) 2004, France, Toulouse, 5–7 July 2004. Proceedings on CD.

[18] Elizarova T.G., Kalachinskaya I.S., Sheretov Yu.V.: Separating flow behind a back-step. Part I. Quasi-hydrodynamic equations and computation of a laminar flow. http://arXiv.org/abs/math-ph/0407053 (2004).

[19] Landau L.D., Lifshitz E.M.: Hydrodynamics, Ed. Nauka, Moscow, 1986 (in Russian)